Supplemental Information

Force Spectroscopy with 9-μs Resolution and Sub-pN Stability by Tailoring AFM Cantilever Geometry

Devin T. Edwards, Jaevyn K. Faulk, Marc-André LeBlanc, and Thomas T. Perkins

Supporting Information

Force Spectroscopy with 9-µs Resolution and Sub-pN Stability by Tailoring AFM Cantilever Geometry

Devin T. Edwards,[1] Jaevyn K. Faulk,[1] Marc-André LeBlanc,[2] and Thomas T. Perkins[1,3,*]

[1]JILA, National Institute of Standards and Technology and University of Colorado, Boulder, Colorado 80309, USA; [2]Department of Chemistry and Biochemistry, [3]Department of Molecular, Cellular, and Developmental Biology, University of Colorado, Boulder, Colorado 80309, USA;

MATERIALS & METHODS:

SUPPORTING FIGURES & TABLES:

MATERIALS & METHODS:

FIB MODIFICATION OF CANTILEVERS

Cantilever selection: To accurately compare cantilever performance due to difference in modifications, we wanted to start with cantilevers that exhibited the same mechanical properties. To do so, we selected ~15 cantilevers from two commercial packs for pre-calibration. The stiffness of each cantilever was then determined in air, as described in detail below. We next recorded the thermal motion of the cantilever in liquid after positioning it 50 nm from the surface. From this data, we calculated the force power spectral density (PSD) for each lever. We next selected for modification a subset of the measured cantilevers that exhibited similar stiffnesses (k), characteristic frequencies (f_c), and quality factors (Q). The k and PSD for each of the 3 modified cantilevers used in the main manuscript are shown in Fig. S3. While in this present work we focused on comparing the performance of these three cantilevers along with an unmodified cantilever, we have made tens to hundreds of Warhammers and Mod Minis, respectively.

FIB modification: Each of the three modified cantilevers followed a similar FIB protocol, with small differences noted below. In general, we used a previously published step-by-step protocol for fabricating a Modified BioLever Mini (*i.e.*, "Mod Mini") (1). Briefly, as diagrammed in Fig. S4 A, we first used a defocused ion beam to etch a rectangular trench of 8×12 μm^2 at the end of the cantilever by milling only through the gold and chromium capping layer. Next, we used a tightly focused ion beam to cut three sides of a rectangle through the cantilever. The two cuts along the length of the cantilever extend slightly onto the supporting chip. This step left two ~1 μm-wide supporting "legs." In the next cut, we cut along the base of the cantilever connecting the two cuts along the long axis of the cantilever. This cut caused a rectangular "flap" to fold up. Next, to further reduce k and eliminate FIB-induced bending of the cantilever, we simultaneously thinned both the legs. We then coated the rectangular patch defined by the shallow trench at the end of the cantilever with tetraethyl orthosilicate (TEOS) using electron-beam-induced deposition. This process resulted in a transparent capping layer that protected the coated region during a subsequent pair of wet chemical etches that sequentially removed the gold and underlying chromium layers. The trench, not used in our original FIB-modification protocol (2), helped ensure that the TEOS layer firmly adhered to the silicon nitride cantilever and thereby prevented undercutting of the gold and chromium during the wet chemical etch.

To make a Long-cut Mini (Fig. S4 B), we used a nearly identical protocol. The only distinction is that the TEOS trench was 4×4 μm^2, allowing the rectangular flap to extend to ~5 μm from the end of the cantilever.

To make a Warhammer cantilever (Fig. S4 C), we started with the same size TEOS frame as the long-cut Mini. However, instead of cutting out the rectangular frame, we instead cut around either side of the TEOS trench and all the way back to the cantilever chip, leaving only a single 2-μm-wide central supporting shaft. We then cut these outer flaps along the base of the cantilever,

which caused them to bend upwards and out of the way. The rest of the modification process then preceded as with the other cantilevers. We note that these flaps either remained attached to the chip after immersion in liquid or detached. Only very rarely did the flaps interfere with the use of a cantilever. We also note that we found that the back side of the cantilever directly above the tip did not contribute to the reflected laser light (*i.e.*, sum signal on the QPD) when it was gold coated. Hence, in our final design, we did not leave this area gold-coated.

AFM INSTRUMENTATION

AFM: We collected our data on a Cypher ES AFM (Asylum Research) and used its temperature controlled, closed fluidic cell to maintain 25 °C, except as noted. To detect the cantilevers, we used two detection modules available from Asylum Research that had different spot sizes: a standard-spot-size laser diode (30×10 μm^2) and a small-spot-size super-luminescent diode (SLD) (9×3 μm^2). The commercial small-spot-size module detected modified cantilevers with no loss in force precision across the full measured bandwidth (Fig. S2 A) as compared to a previously described, custom-built detection system that featured an even smaller spot size (3-µm-diameter) (3). For completeness, we note that this custom unit now also utilizes an SLD instead of a laser diode, since it led to a decrease in an optical-interference artifact when detecting a Warhammer cantilever (Fig. S2 B). Such an artifact is common when detecting an ultrashort cantilever ($L = 9$ µm) (4). We measured the spot profile of the commercial small-spot-size module (Fig. S2 C) and that of our circular-small-spot module (Fig. S2 D). To do so, we placed a 1-µm diameter iris on top of a photodiode in our commercial AFM. Then, without a cantilever installed, we focused the detection laser onto the surface and used the AFM to scan the iris through the laser beam while recording the photodiode voltage.

To reduce optical-interference artifacts for users of the commercial small spot size module, we developed a variant of the Warhammer—an extended Warhammer (Fig. S2 E)—that used a slightly narrower but longer reflective region (2.7×7.4 μm^2) than our standard one (4×4 μm^2) (Fig. S2 F) that better matched the spot size of the commercial unit. As expected, this variant significantly reduced the optical-interference artifact (Fig. S2 B, orange vs. purple, respectively) at minimal reduction in f_c (16 vs 19 kHz, respectively) (Fig. S2 A). Finally, we emphasize that even much larger interference fringes do not interfere with biological interpretation of AFM-based SMFS and, hence users can take full advantage of the performance gains afforded by a standard Warhammer and then computationally subtract out the interference artifact in post-processing of the data. Indeed, we have previously computationally subtracted out much larger interference artifacts of ~400 pN peak-to-peak that arose when applying FIB-modified ultrashort cantilevers ($L = 9$ µm) (5).

Cantilever characterization: To determine k, we measured the cantilever's stiffness in air since the Q of the cantilever was higher. We first determined detection sensitivity (nm/V) by pressing the cantilever into hard contact with a mica or cleaned glass surface. A surface indentation of at

least 500 pN was used to achieve a linear force-vs-position curve, and the sensitivity was determined from a fit to the linear portion of this indentation curve. We then retracted the cantilever until it was >1 μm from the surface. Next, we measured the cantilever's thermal motion at high bandwidth (typically 2 MHz) and fit the first harmonic of the resulting PSD (6). This process was repeated at least 3 times in different spots around the surface. The resulting values of k were averaged to assign a k to a cantilever. Subsequently, all measurements in fluid utilized this k as a known constant and analyzed the PSD in liquid to determine the sensitivity, in analogy with a calibration protocol developed for ultrashort cantilevers (4). In general, if thermal calibration is performed in liquid, the resulting probe stiffness agrees to within ±15% of the stiffness determined in air.

To provide insight into a cantilever's performance in single-molecule assays, we next calculated two metrics. To do so, we let the cantilever settle for ~2 h after mounting and immersion in liquid. We next positioned the cantilever 50 nm above the surface to account for increased hydrodynamic drag near a surface (*i.e.*, squeezed film damping in the language of the AFM instrumentation community) and then recorded the thermal motion of the cantilever for ~100 s at 500 kHz. For these measurements, the X-, Y-, and Z- feedback loops on the AFM were engaged to hold the AFM chip at a constant location above the surface. From these records, we computed force PSDs. To reduce noise in the spectrum, we divided the traces into ~20 shorter traces and then averaged the PSDs from these short traces. The same 100 s trace was used to calculate the force precision, strictly the Allan deviation: $\sigma_F(T) = \sqrt{\frac{1}{2}\langle(\bar{F}_{i+1} - \bar{F}_i)^2\rangle_T}$, where F_i is the mean value of the data over the ith time interval of T duration (7). One of the virtues of the Allan deviation is it shows on what timescale increased averaging of Brownian motion over longer periods for improved force precision becomes limited by instrumental noise.

Improved sub-pN force stability by increased settling time: Prior work from our lab showed that we could achieve sub-pN performance 30 min after mounting the cantilever in liquid when measuring an Olympus BioLever Long ($k \approx 7$ pN/nm) that had had its metallic coating removed (8). With the Warhammer geometry, we observed sub-pN force precision, as measured by the Allan deviation, at 100 s typically 1 h after mounting. While longer than for an uncoated BioLever Long, it is still a rather minimal settling time by AFM-based SMFS standards. That said, not every cantilever exhibited this level of stability. However, standard Mod. Mini cantilevers with similar k consistently achieved a sub-pN Allan deviation at 100 s under similar conditions (2). To account for this variation, we measure the Allan deviation ~1 h after mounting to determine the suitability of a particular cantilever when needing the highest level of force stability.

Ongoing work is trying to determine the origin of these differences between individual cantilevers. Somewhat unexpectedly, we observed force stability varied with the precise vertical position of the detector beam focus relative to the cantilever when measuring the same Warhammer cantilever (Fig. S5 A). The detailed mechanism leading to this result remains under investigation.

On usability, we note that slight defocusing of the cantilever reduces the optical-interference artifact but degrades force stability. Given our prior success in computationally subtracting out even large optical-interference artifacts (5), we recommend positioning the beam waist of the detector beam in the plane of the cantilever (though this recommendation may vary for different AFMs).

To investigate if extended settling times could further improve force stability, we measured the force precision as a function of averaging time at 4 h and 14 h after mounting in liquid. In particular, we had achieved 0.5 pN stability at 100 s when letting the cantilever settle for 14 h, about a two-fold improvement over what we measured at 4 h (Fig. S5 B). We note that one advantage of our commercially available, temperature-regulated sample holder is that this level of stability can be achieved while holding the biological sample at 4 °C during the overnight settling period and then warming it up for use the following morning. Hence, this level of stability should be available even for temperature-sensitive samples. Finally, we note that these results suggest that force instability was more closely associated with immersion of the cantilever through the air-water interface, rather than the temperature history of the cantilever.

SINGLE-MOLECULE ASSAY

Coverslip and AFM tip functionalization: To improve the quality of our AFM data, we site-specifically stretched our polyprotein construct between a polyethylene glycol (PEG)-coated glass coverslip and AFM tip (9). In this scheme, we labeled the biomolecule of interest using a biotin moiety at one end and dibenzocyclooctyne (DBCO), a copper-free click reagent, at the other end. This scheme allowed us to couple the labeled polyprotein to an azide-functionalized coverslip and then stretch it using a streptavidin-coated AFM tip. We functionalized coverslips with a short silane-PEG-azide reagent (PG2-AZSL-600, Nanocs Inc), as previously detailed (9). To make streptavidin-coated AFM tips, we first functionalized the silicon-nitride tips using a silane-PEG-maleimide reagent (PG2-MLSL-600, Nanocs Inc). After rinsing, we then reacted the cantilevers with thiol-derivatized streptavidin (SAVT, Protein Mods LLC). Protein-coated coverslips and AFM tips were stored in PBS [10 mM phosphate buffer (pH 7.4), 140 mM NaCl, 3 mM KCl] at 4 °C prior to use and could be reused over multiple days.

Polyprotein construct: For our site-specific coupling scheme, we used a labeled polyprotein construct containing four repeats of NuG2, as recently described (9). Briefly, NuG2 served as a marker protein to assure only individual molecules were analyzed. NuG2 is a fast-folding variant of GB1 (10) and well-characterized by AFM (11,12). We embedded the protein of interest—α_3D or calmodulin—into the middle of this construct. Because none of these proteins contained an internal cysteine, we labeled the polyprotein via two cysteines positioned near the N- and C-terminals of the polyprotein (as opposed to converting them to aldehydes using an enzymatic reaction) (9). To functionalize with both DBCO and biotin, we reacted the polyprotein with a 10-fold molar excess of both sulfo-maleimide-PEG$_4$-DBCO (Click Chemistry Tools) and maleimide-

biotin (Sigma) overnight at room temperature. While only a fraction of the constructs will be orthogonally labeled with biotin and DBCO, only these constructs were efficiently stretched between an azide-functionalized surface and a streptavidin-coated AFM tip.

After purifying away the unreacted reagents, this labeled polyprotein was deposited onto azide-functionalized glass coverslips. The deposited surfaces were incubated at 4 °C overnight in simple humidity chambers. Immediately prior to AFM assays, we repeatedly washed the coverslips by pipetting 1 mL of buffer over the sample (held at ~45 degrees) a minimum of 10 times. Care was taken to avoid dewetting the surface during rinsing. For the α_3D assay, we rinsed and performed the experiment in a buffer of 50 mM sodium phosphate (pH 7.0) and 150 mM NaCl. For the calmodulin assay, we first rinsed in 50 mM TrisHCl (pH 8.0) and 150 mM KCl and then rinsed with at least 3 mL of 50 mM TrisHCl (pH 8.0), 150 mM KCl, and 10 mM $CaCl_2$. The calmodulin AFM assays were performed in this calcium-containing buffer. Note, the initial rinsing in the absence of $CaCl_2$ avoids the known precipitation of phosphate buffers by $CaCl_2$ before introducing the $CaCl_2$ needed study the properly folded calcium-binding protein calmodulin.

Data-acquisition protocol for protein-unfolding assays. We used a multi-step process to measure the temporal resolution of the cantilever during a single-molecule assay. As illustrated in Fig. S6 A, we initially gently pressed the tip into the surface at ~150 pN for 1 s to promote attachment between the streptavidin-coated tip and the biotin-labeled polyprotein. We then retracted the tip from the surface at 400 nm/s until a force of 40 pN was reached at a tip-sample separation of at least ~80 nm (Fig. S6 B, red curve). This real-time triggering scheme selected for molecules attached to the cantilever while suppressing triggering on surface adhesion. Upon detection of a candidate molecule, we returned the cantilever to within 5 nm of the surface (*i.e, F $\approx$ 0 pN*) (Fig. S6 B, purple curve) and paused for 1 s to promote refolding. We next stretched the polyprotein to a predetermined extension based on the location of the first NuG2 unfolding event and only analyzed traces in which α_3D and three of the four NuG2 domains unfolded but the fourth NuG2 domain remained folded (Fig. S6 C). We then moved the cantilever to apply 80 pN across the polyprotein and then held the cantilever stationary (*v* = 0 nm/s) for 1 s during which the final NuG2 domain unfolded (Fig S6 D). Following this unfolding event, we lowered the tip again to within 5 nm of the surface for 1 s to promote refolding and then retracted the cantilever at *v* = 400 nm/s to unfold the entire polyprotein and detach it from the tip (Fig. S6 E). This final unfolding event ensured that the analyzed events arose from single polyproteins. We recorded the cantilever deflection at several different data-acquisition rates during this process. Specifically, we measured at 5 kHz during Fig. S6 B, while the second retraction and final retraction were recorded at 50 kHz (Fig. S6 C, E). To determine the cantilever response at high-time resolution, we concurrently sampled the second retraction and subsequent pause (Fig. S6 C, D) at 50 kHz and 500 kHz.

We used a simpler data-acquisition protocol for the calmodulin assay. As with α_3D assay, we first used a real-time trigger to select for a connection by retracting the cantilever at 400 nm/s until the *F* = 40 pN at a tip-sample separation of at least ~80 nm. Upon detection of a candidate

molecule, we again returned the cantilever to within 5 nm of the surface and paused for 1 s to promote refolding. We next retracted the tip at either 100 nm/s for the calmodulin-alone assay (Fig. 3 A, B) or 400 nm/s for calmodulin unfolding in the presence of myosin light chain kinase (Fig. 3 C). The initial retraction and refolding were digitized at 5 kHz, while the final retraction was recorded at 50 kHz. For samples containing the myosin light chain kinase peptide (GenScript, Calmodulin Binding Peptide 1, RP13247), it was introduced at 1 μM concentration.

DATA ANALYSIS

Protein data: The smoothing of each data set is noted in figure captions. For data recorded at 50 kHz, we applied a 2nd-order Savitsky-Galoy filter to the data. When an n-point smoothing filter is applied, we report the smoothed bandwidth as the original sampling frequency divided by n. For the high-bandwidth data recorded at 500 kHz, we applied a digital narrowband (300 Hz) notch filter at 125 kHz. This filter removes a known drive frequency in our AFM that occasionally contributes noise to the measurement. For the data smoothed to 5 kHz in Fig. S1, we applied a digital low-pass filter with a passband ending at 5 kHz.

Although the cantilever geometries preserved high laser reflectivity, small interference artifacts remained and needed to be computationally removed. We removed these optical-interference artifacts in a post-processing step, as described previously (3). Briefly, we used a heuristic model to describe the sine-wave-like interference artifact:

$$V_d = A_1 + A_2 \cdot Z_{PZT} + (A_3 + A_4 \cdot Z_{PZT}) \cdot \sin[A_5 + A_6 \cdot Z_{PZT}]$$

Where V_D is the deflection voltage, Z_{PZT} is the Z-stage position sensor, and A_1, A_2, A_3, A_4, A_5, A_6 are fit parameters that are determined from the approach portion of the trace. This model then allows us to correct the retraction curves to eliminate the contribution from the interference artifact.

We analyzed the resulting force-extension curves (FECs) using an improved numerical approximation for an inextensible worm-like chain (WLC) model (13). FECs for a wide variety of biopolymers including DNA and proteins have been well described by a WLC model. The WLC model is parameterized by the persistence length (p) and contour length (L_0) of the polymer. In our fits, we used $p = 0.4$ nm, a common value for AFM-based SMFS. As each protein domain in the polyprotein unfolded, the contour length should increase by a fixed length (ΔL_0) proportional to the number of the released amino acids. As shown in Figure S7, the FECs measured with modified cantilevers were well described by WLC fits.
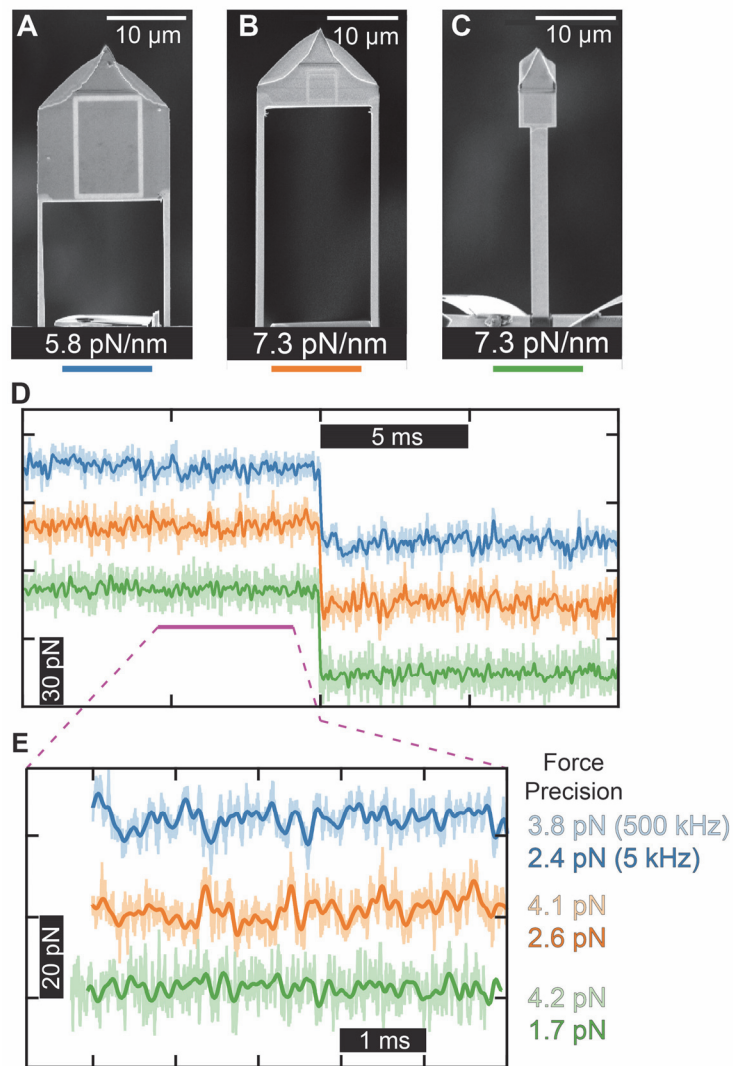
Figure S1: Improved force precision visualized in the time domain. (A-C) SEM image and k of the modified cantilevers shown in Fig. 1,2. Color below the image corresponds to the traces shown in panels (D) and (E). (D) High-bandwidth force-vs-time traces showing the unfolding of the fourth NuG2 domain at $v = 0$ nm/s. Data taken from Fig. 2 B. Filtering for the light and dark colored traces are 500 and 5 kHz, respectively. (E) Force-vs-time trace immediately before the rupture of the fourth NuG2 domain. The RMS force precision for each trace is shown to the right using the same smoothing as in panel (D).
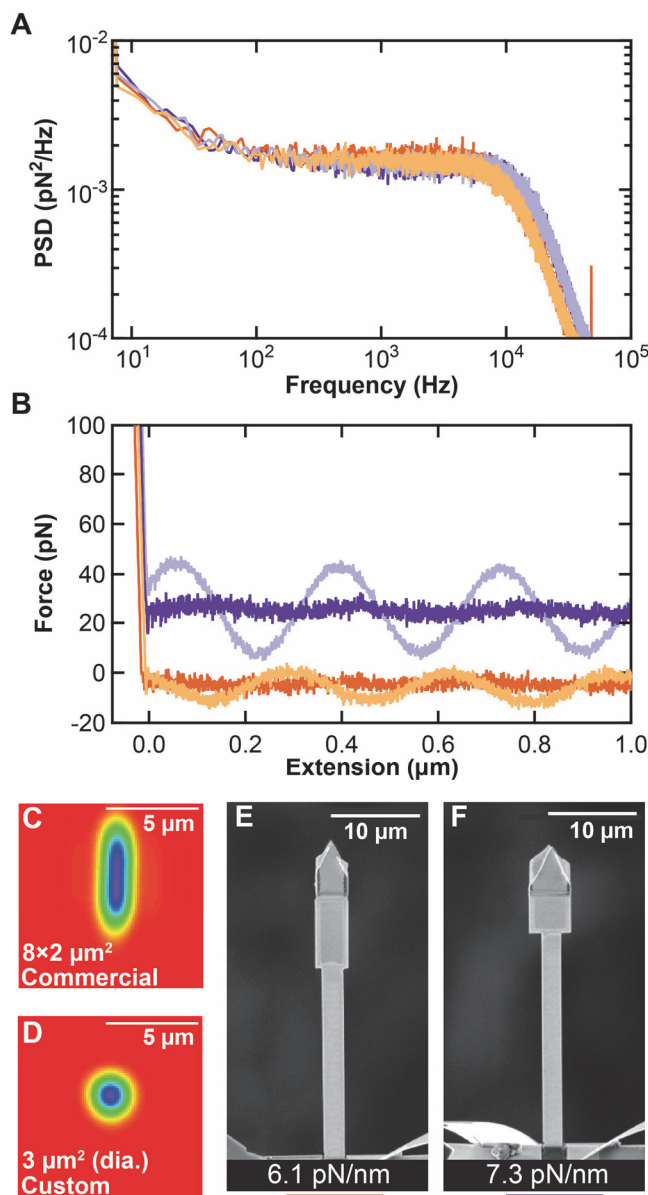
Figure S2: Detecting Warhammers with a commercial-detection module. (A) Force power spectral density (PSD) of the standard (purple) and extended Warhammer (orange). The darker color traces were taken using a custom detection module (3-µm-dia) while the lighter color traces were taken with the commercial small-spot-size module. The overlap of the PSDs shows no change in measured precision over all f between the different detection modules. (B) Force-extension traces show the optical-interference artifact for the standard (purple) and an extended (orange) Warhammer geometry. (C,D) Measured spatial distribution of the spot size formed by the commercial and custom detection modules. (E,F) SEM images (prior to gold etching) of an extended and normal Warhammer style cantilever showing the lengthened yet narrowed reflective patch (7.4×2.7 µm^2) for an extended Warhammer relative to a standard patch (4×4 µm^2). The extend geometry reduced the optical-interference artifact when using the commercial small-spot-size module as shown in panel B with minimal change in f_c (16 kHz vs 19 kHz, respectively).
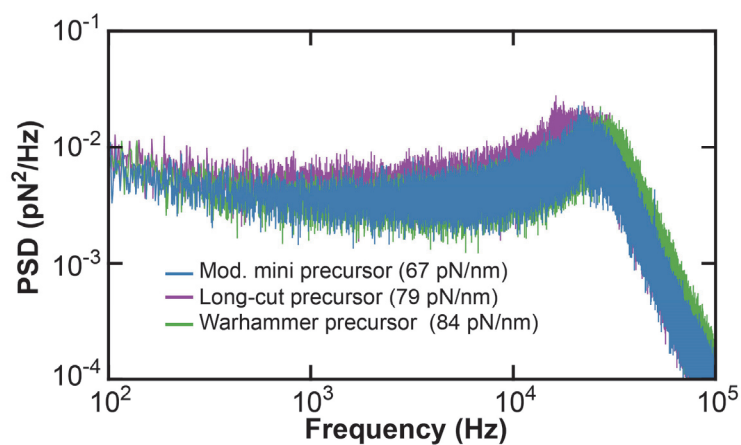
Figure S3: Mechanical properties of the compared cantilevers prior to modifications. Force power spectral density (PSD) in liquid plotted as a function of frequency for three modified BioLever Minis shown in Figure 1 and 2 prior to their modification. The *k* of each cantilever determined in air is listed. These three cantilevers were chosen for modification due to the similarity of their mechanical properties (*i.e*, *k, Q,* and PSD) to facilitate comparison.
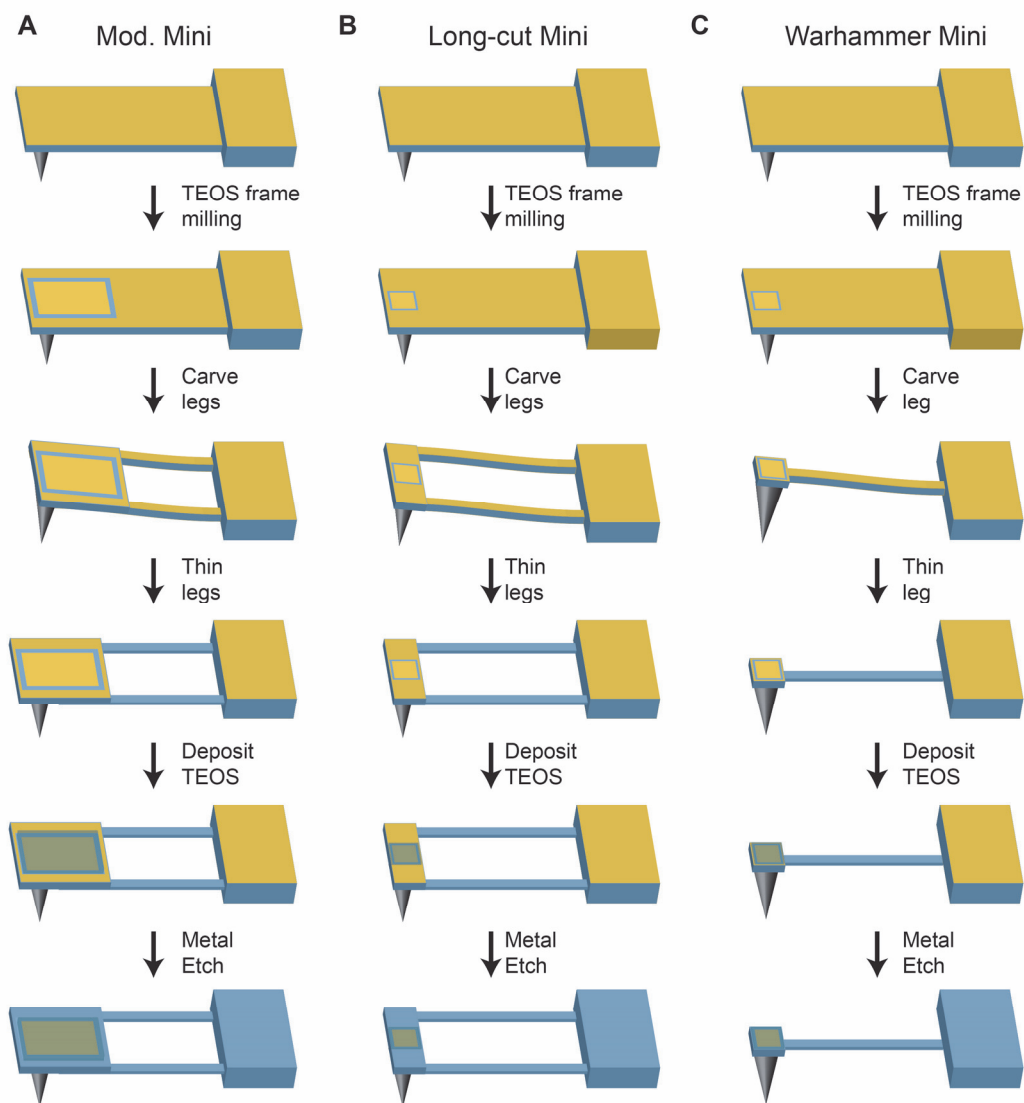
Figure S4: Cantilever modification protocol. A cartoon depiction of the process for focused-ion beam (FIB) modification of the three cantilever geometries investigated: (A) a Mod Mini, (B) a Long-cut Mini, and (C) a Warhammer. The general process for each cantilever geometry consisted of five processing steps: TEOS framing, carving out the legs, thinning the legs, depositing the TEOS, and a wet etch to remove the gold and underlying chromium layers.
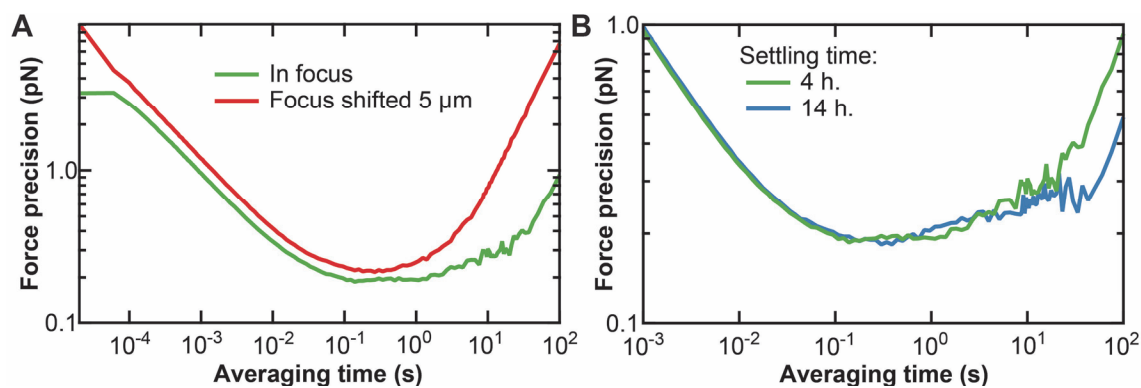
Figure S5: Improved long-term stability. (A) Variation in measured force precision over a given averaging time when changing the vertical position of the detector focus for a Warhammer in liquid positioned 50 nm over the surface. Specifically, measured long-term stability was significantly degraded (red) when the focus was shifted 5-μm vertically upward from the visible sharp focus. (B) Improvement in measured force precision over long periods when the cantilever was allowed to settle overnight versus 4 h (blue vs. green respectively).
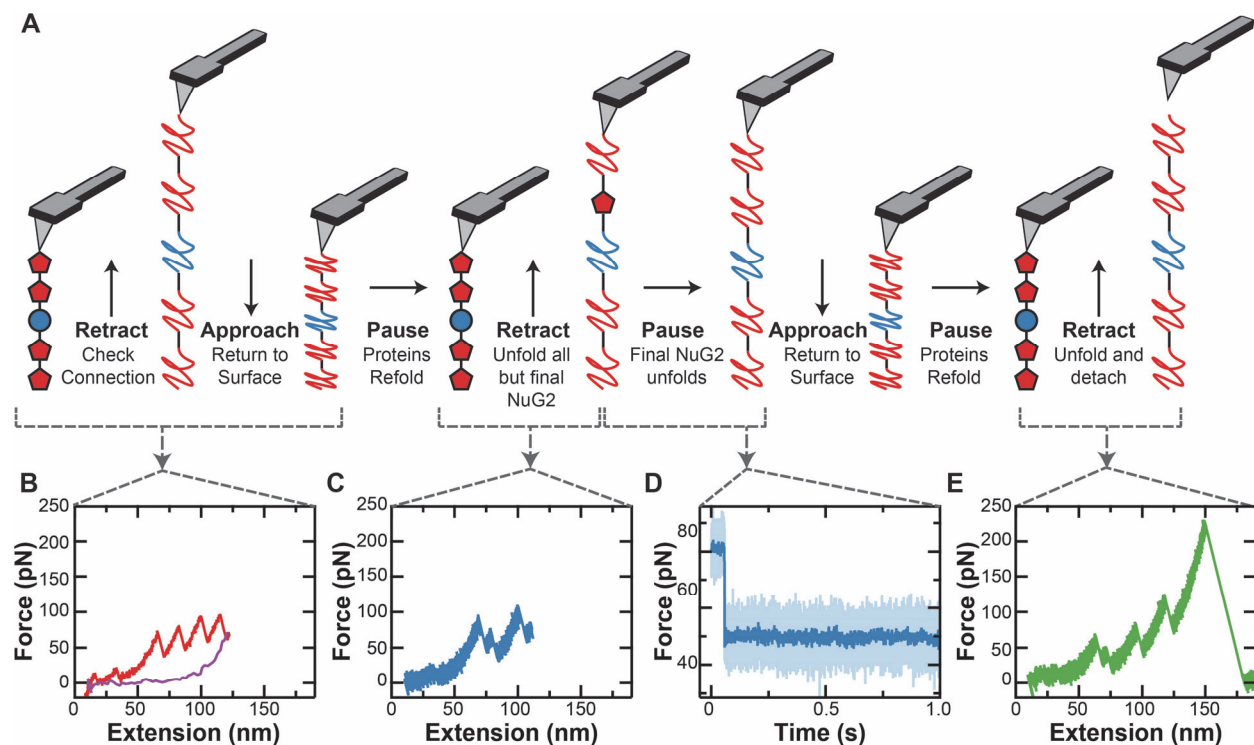
Figure S6: Multi-step unfolding protocol for measuring temporal response during a protein-unfolding assay. (A) A pictorial description of the unfolding protocol used to observe unfolding of a single NuG2 from a predetermined force. The four domains of NuG2 are depicted in red while the single domain of α_3D is shown in blue. Geometric shapes (pentagons and circles) represent folded domains while a linear depiction represents an unfolded domain. (B) Force-extension curve (FEC) shows the initial unfolding (red) of the polyprotein at $v = 400$ nm/s up to force (40 pN) and extension (>80 nm) values recognized by a real-time trigger scheme that selects for a promising candidate molecule. After triggering, the tip was then returned to the surface, resulting in a second FEC (purple). (C) FEC showing the stretching of the polyprotein to an extension leading to 80 pN of applied force and followed by the unfolding of the remaining single NuG2 domain. (D) Force-vs-time plot during a pause at constant stage position ($v = 0$ nm/s) (blue), during which the final NuG2 domain unfolded. (E) FEC showing the final unfolding curve after letting the polyprotein refold at $F \approx 0$ pN for 1 s. This final FEC shows all four NuG2 domains and the α_3D domain unfold, assuring a single polyprotein was measured. Data in panels B, C, and E filtered to 50 kHz. Data in panel D filtered to 50 kHz (light blue) and 1 kHz (dark blue).
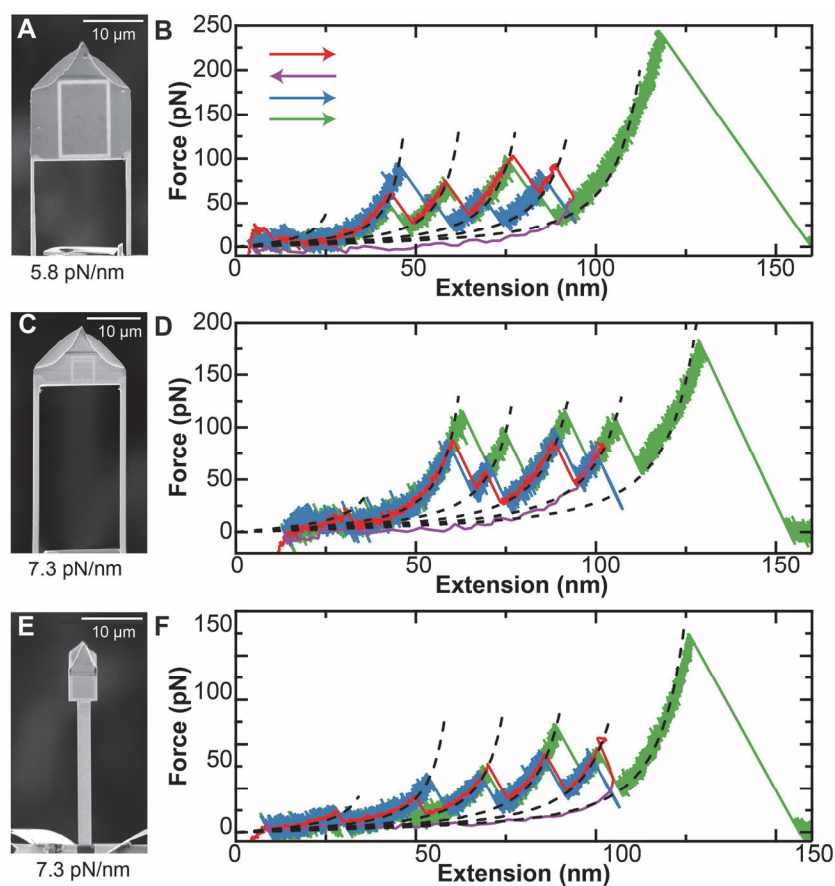
Figure S7: Protein-unfolding data well modeled by WLC fits. (A) An SEM image of a modified BioLever Mini, with its measured stiffness. (B) Force-extension curves acquired during the multi-step unfolding protocol (Fig. S6) used to determine the cantilever response for the cantilever shown in panel A. Red and purple traces represent the first unfolding and refolding step, respectively (Fig. S6 B). The blue trace shows the unfolding of α_3D and four domains of NuG2 (Fig. S6 C, D). The green trace shows the final unfolding record after allowing the protein to refold for 1 s at $F \approx 0$ pN. (C) An SEM image of a Long Cut Mini. (D) FEC acquired using the Long Cut Mini shown in panel C, with the same color coding as in B. (E) An SEM image of a Warhammer. (F) FEC acquired using the Warhammer shown in panel E with the same color coding as in B. Data in red and purple acquired at 5 kHz, data in blue and green acquired at 50 kHz.

REFERENCES

1. Faulk, J. K., D. T. Edwards, …, T. T. Perkins. 2017. Improved force spectroscopy using focused-ion-beam-modified cantilevers. *Methods Enzymol.* 582:321-351.
2. Bull, M. S., R. M. Sullan, …, T. T. Perkins. 2014. Improved single molecule force spectroscopy using micromachined cantilevers. *ACS Nano* 8:4984-4995.
3. Edwards, D. T., J. K. Faulk, …, T. T. Perkins. 2015. Optimizing 1-μs-resolution single-molecule force spectroscopy on a commercial atomic force microscope. *Nano Lett.* 15:7091-7098.
4. Rico, F., L. Gonzalez, …, S. Scheuring. 2013. High-speed force spectroscopy unfolds titin at the velocity of molecular dynamics simulations. *Science* 342:741-743.
5. Yu, H., M. G. Siewny, …, T. T. Perkins. 2017. Hidden dynamics in the unfolding of individual bacteriorhodopsin proteins. *Science* 355:945-950.
6. Proksch, R., T. E. Schaffer, …, M. B. Viani. 2004. Finite optical spot size and position corrections in thermal spring constant calibration. *Nanotechnology* 15:1344-1350.
7. Sullivan, D. B., D. W. Allan, …, E. L. Walls, editors. 1990. Characterization of Clocks and Oscillators. U.S. Government Printing Office, Washington.
8. Churnside, A. B., R. M. Sullan, …, T. T. Perkins. 2012. Routine and timely sub-picoNewton force stability and precision for biological applications of atomic force microscopy. *Nano Lett.* 12:3557-3561.
9. Walder, R., M.-A. LeBlanc, …, T. T. Perkins. 2017. Rapid characterization of a mechanically labile α-helical protein enabled by efficient site-specific bioconjugation. *J. Am. Chem. Soc.* 139:9867–9875.
10. Nauli, S., B. Kuhlman, and D. Baker. 2001. Computer-based redesign of a protein folding pathway. *Nat. Struct. Biol.* 8:602-605.
11. Cao, Y., M. M. Balamurali, …, H. B. Li. 2007. A functional single-molecule binding assay via force spectroscopy. *Proc. Natl. Acad. Sci. U.S.A.* 104:15677-15681.
12. He, C., C. Hu, …, H. Li. 2015. Direct observation of the reversible two-state unfolding and refolding of an alpha/beta protein by single-molecule atomic force microscopy. *Angew. Chem. Int. Edit.* 54:9921-9925.
13. Bouchiat, C., M. D. Wang, …, V. Croquette. 1999. Estimating the persistence length of a worm-like chain molecule from force-extension measurements. *Biophys. J.* 76:409-413.